Different Influencing Mechanisms of Two ENSO Types on the Interannual Variation in Diurnal SST over the Niño-3 and Niño-4 Regions

XIAODAN YANG,[a,b,c] YAJUAN SONG,[a,b,c] MENG WEI,[a,b,c] YUHUAN XUE,[a,b,c] AND ZHENYA SONG[a,b,c]

[a] *First Institute of Oceanography and Key Laboratory of Marine Science and Numerical Modeling, Ministry of Natural Resources, Qingdao, China*

[b] *Laboratory for Regional Oceanography and Numerical Modeling, Qingdao National Laboratory for Marine Science and Technology, Qingdao, China*

[c] *Shandong Key Laboratory of Marine Science and Numerical Modeling, Qingdao, China*

(Manuscript received 25 October 2020, in final form 24 September 2021)

ABSTRACT: In this paper, the different effects of the eastern equatorial Pacific (EP) and central equatorial Pacific (CP) Ocean El Niño–Southern Oscillation (ENSO) events on interannual variation in the diurnal sea surface temperature (SST) are explored in both the Niño-3 and Niño-4 regions. In the Niño-3 region, the diurnal SST anomaly (DSSTA) is negative during both EP and CP El Niño events and becomes positive during both EP and CP La Niña events. However, the DSSTA in the Niño-4 region is positive in El Niño years and negative in La Niña years, which is opposite to that in the Niño-3 region. Further analysis indicates that the incident shortwave radiation (SWR), wind stress (WS), and upward latent heat flux (LHF) are the main factors causing the different interannual variations in the DSST. In the Niño-3 region, decreased SWR and increased LHF lead to a negative DSSTA in EP El Niño years, and enhanced WS and increased LHF cause a negative DSSTA in CP El Niño years. Conversely, in that same region, increased SWR and decreased LHF lead to a positive DSSTA in EP La Niña years, and reduced WS and decreased LHF cause a positive DSSTA in CP La Niña years. In the Niño-4 region, the reduced trade wind plays a key role in producing the positive DSSTA, whereas the decreased SWR has an opposite effect that reduces the range of the DSSTA during both EP and CP El Niño events, and conversely the enhanced trade wind plays a key role in producing the negative DSSTA, whereas the increased SWR has an opposite effect that increases the range of the DSSTA during both EP and CP La Niña events.

KEYWORDS: Diurnal effects; Sea surface temperature; Wind; ENSO; Shortwave radiation; Interannual variability

1. Introduction

Sea surface temperature (SST) plays a principal role in air–sea interactions, because it is necessary for the estimation of the air–sea heat fluxes, including the sensible and latent heat and upward longwave radiation. SST variations (or errors) of a magnitude of 1°C can have an important impact on air–sea interactions, especially when the surface temperature is high. A 1°C bias in SST would result in 27 W m^{-2} errors in the net surface heat flux in the tropical western Pacific (Webster et al. 1996). Furthermore, calculating the heat balance in the upper ocean to an accuracy of 10 W m^{-2} requires accuracy of ±0.2°C in SST (Fairall et al. 1996b).

The diurnal variation in SST, which is caused by solar radiation and Earth's rotation, constitutes one of the SST's primary variations. Under calm and clear conditions, the diurnal SST amplitude (DSST) could exceed 3°C (Fairall et al. 1996a; Soloviev and Lukas 1997; Kawai and Wada 2007; Gentemann et al. 2008; Yang et al. 2017). Ignoring the diurnal SST variation will lead to large errors in SST simulations. Thus, the study of the DSST and its variations is very important and will contribute to a better understanding of the air–sea interaction in tropical regions (Clayson and Bogdanoff 2013).

The mean state and seasonal variation of the DSST have been widely discussed in previous studies (e.g., Stuart-Menteth et al. 2003; Clayson and Weitlich 2007; Kawai and Wada 2007; Yang et al. 2015; Zhang et al. 2016). Recently, the interannual variation in the DSST under ENSO events has been attracting increasing attention. By analyzing the DSST estimated using parameterization from 1996 to 2000, Clayson and Weitlich (2005) found a DSST dipole pattern in the western and eastern equatorial Pacific influenced by the 1997/98 El Niño event and the 1998/99 La Niña event. During El Niño events, in the eastern equatorial Pacific (EP) region, the DSST significantly decreased as a result of decreased peak shortwave radiation (SWR) and increased winds and conversely significantly enhanced as a result of increased peak SWR and reduced winds during La Niña events, similar to that discussed in Cronin and Kessler (2002). Using the 31-yr modeling results, Li et al. (2018) also showed that the DSST in the Niño-3 region (5°N–5°S, 150°–90°W) is dramatically opposite to that of ENSO, with a correlation coefficient of −0.54. In addition, they noted that the strongest positive correlation region is in the central equatorial Pacific (CP), which has a cross correlation between the DSST and the Niño-3 index exceeding 0.7, with a 6-month lead in the DSST.

However, the previous results were obtained using either model results (including parametric model) or short-term observations. Long-term interannual variation in the DSST has not been studied using observations yet. Moreover, previous studies have been based on the canonical ENSO, whereas the tropical Pacific Ocean has begun to experience a new type of El Niño referred to as the CP El Niño (Kao and Yu 2009; Capotondi et al. 2015), which became more common over the

Denotes content that is immediately available upon publication as open access.

Corresponding author: Zhenya Song, songroy@fio.org.cn

DOI: 10.1175/JCLI-D-20-0815.1

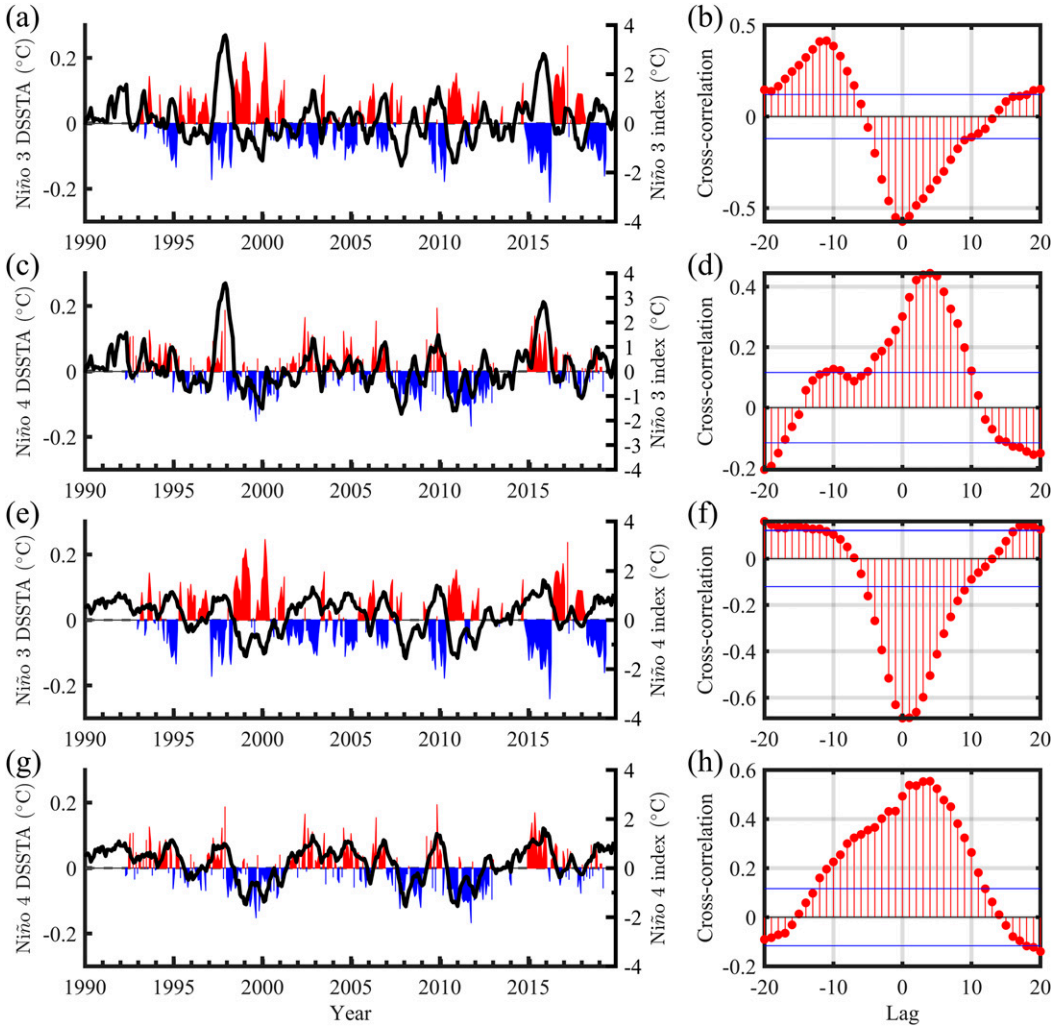

FIG. 1. (a),(c),(e),(g) Comparison of DSSTA (colored fill; red indicates positive values, and blue indicates negative values) with the Niño SST indices (black line) in the Niño-3 and Niño-4 regions from 1990 to 2018, and (b),(d),(f),(h) their cross-correlations (the horizontal blue lines are the upper and lower confidence bounds).

last decade (Lee and McPhaden 2010). The interannual variation in the DSST affected by the CP El Niño has not yet been discussed. In addition, as shown in Li et al. (2018), the responses of the DSST in the EP and CP regions to ENSO events are different. Therefore, the DSST in different regions in the equatorial Pacific should also be considered separately.

Recently, using nearly 29 years of Tropical Atmosphere Ocean/Triangle Trans-Ocean Buoy Network (TAO/TRITON) observation data, we discovered a distinct type of interannual DSST variation in the Niño-3 region (5°N–5°S, 150°–90°W) and in the Niño-4 region (5°N–5°S, 160°E–150°W) (Figs. 1a,c,e,g). The cross-correlation coefficients reveal that the DSST anomaly (DSSTA) in the Niño-3 region is negatively correlated, with a coefficient reaching −0.57 from the Niño-3 SST index and a coefficient of approximately −0.69 from the Niño-4 SST index at zero lag (Figs. 1b,f), whereas the correlation of the DSSTA in the Niño-4 region with the Niño-3 SST index and Niño-4 SST index is positive (with coefficients of approximately 0.44 and 0.55, respectively) with a 3- to 4-month lead (Figs. 1d,h). Therefore, two major questions remain to be explored about the detailed characteristics of the interannual variations in the DSST in these two regions and the main mechanisms of the two types of ENSO that control the different interannual variations. The present paper aims to give reasonable answers to the two questions.

The remainder of this paper is organized as follows. The data and methods used in the study are introduced in section 2. In section 3, the effects of two types of ENSO events on the interannual variations in DSST in the Niño-3 and Niño-4 regions are shown. In addition, the influencing mechanisms are indicated. The discussion and conclusions are given in section 4.

2. Data and methods

a. Data

The observational data used in this study are primarily from the TAO/TRITON array (https://www.pmel.noaa.gov/tao/drupal/disdel/),

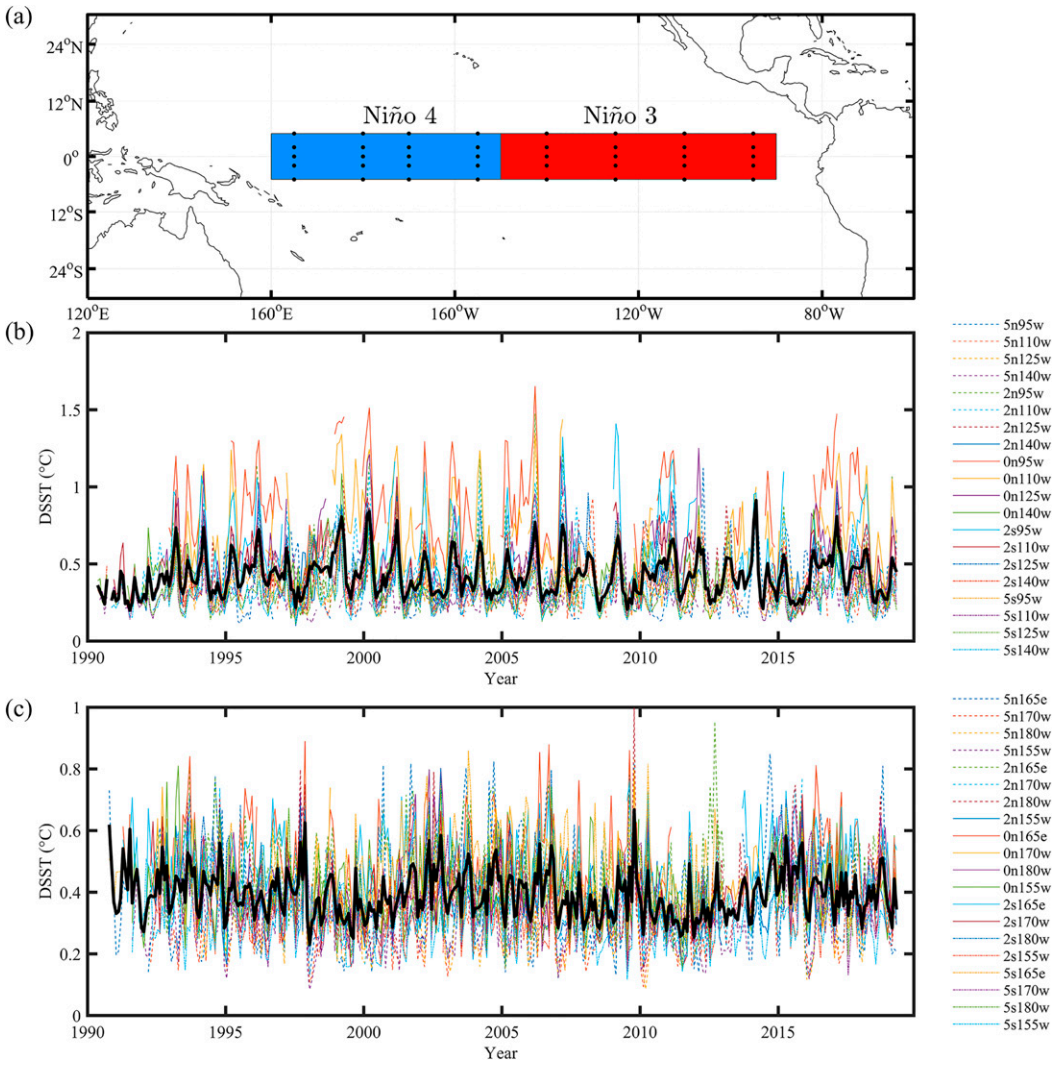

FIG. 2. (a) Locations of the TAO/TRITON buoys, and the monthly mean DSST values (>20 days available in each month) in the (b) Niño-3 and (c) Niño-4 regions. Black lines in (b) and (c) are the ensemble means of DSST when more than 10 buoy observations exist at that time.

which consists of 67 moorings in the tropical Pacific between latitudes 8°N and 8°S and longitudes 95°W and 137°E. The TAO/TRITON array was originally designed to improve ENSO monitoring, understanding, and forecasting (McPhaden et al. 1998). In this study, high-resolution (10 min and hourly) SST data measured at a 1-m depth between latitudes 5°N and 5°S and the longitudes 165°E and 95°W in the Niño-3 region and the Niño-4 region were selected from the TAO/TRITON arrays, consisting of data from 20 buoys in each region (i.e., 40 buoys in total; Fig. 2a). Note that the SST data with a 10-min temporal resolution were transformed to hourly resolution by skipping every six steps to maintain data consistency. Then, the hourly SST data were used to calculate DSST ($SST_{daily\text{-}max} - SST_{daily\text{-}min}$) in these two regions (Figs. 2b,c). Standard measurements on all TAO/TRITON moorings also include atmospheric variables, including downward SWR, downward longwave radiation (LWR), surface wind speed, air temperature, relative humidity, precipitation, and sea level pressure, which can be used to estimate the sensible heat flux (SHF), latent heat flux (LHF), and momentum fluxes (Fairall et al. 1996b).

For all TAO/TRITON arrays, mooring failure and vandalism could lead to data gaps in the oceanic data (Figs. 2b,c) and atmospheric data (Fig. 3). DSST is heavily affected by atmospheric variables, especially SWR, LWR and wind, so the SWR and LWR from ERA5 reanalysis data (resolution: 0.25° × 0.25°) are used to replace the observed SWR and LWR. Moreover, the wind from the Cross-Calibrated Multi-Platform (CCMP) (resolution: 0.25° × 0.25°) instead of ERA5 data are used in this study because the mean biases in CCMP winds (Niño-3 region: $-0.14\,m\,s^{-1}$; Niño-4 region: $-0.22\,m\,s^{-1}$) are considerably smaller than those in ERA5 winds (Niño-3 region: $-0.40\,m\,s^{-1}$; Niño-4 region: $-0.85\,m\,s^{-1}$) when compared with buoy observations. This may be because the CCMP data are a combination of the ERA-Interim reanalysis winds

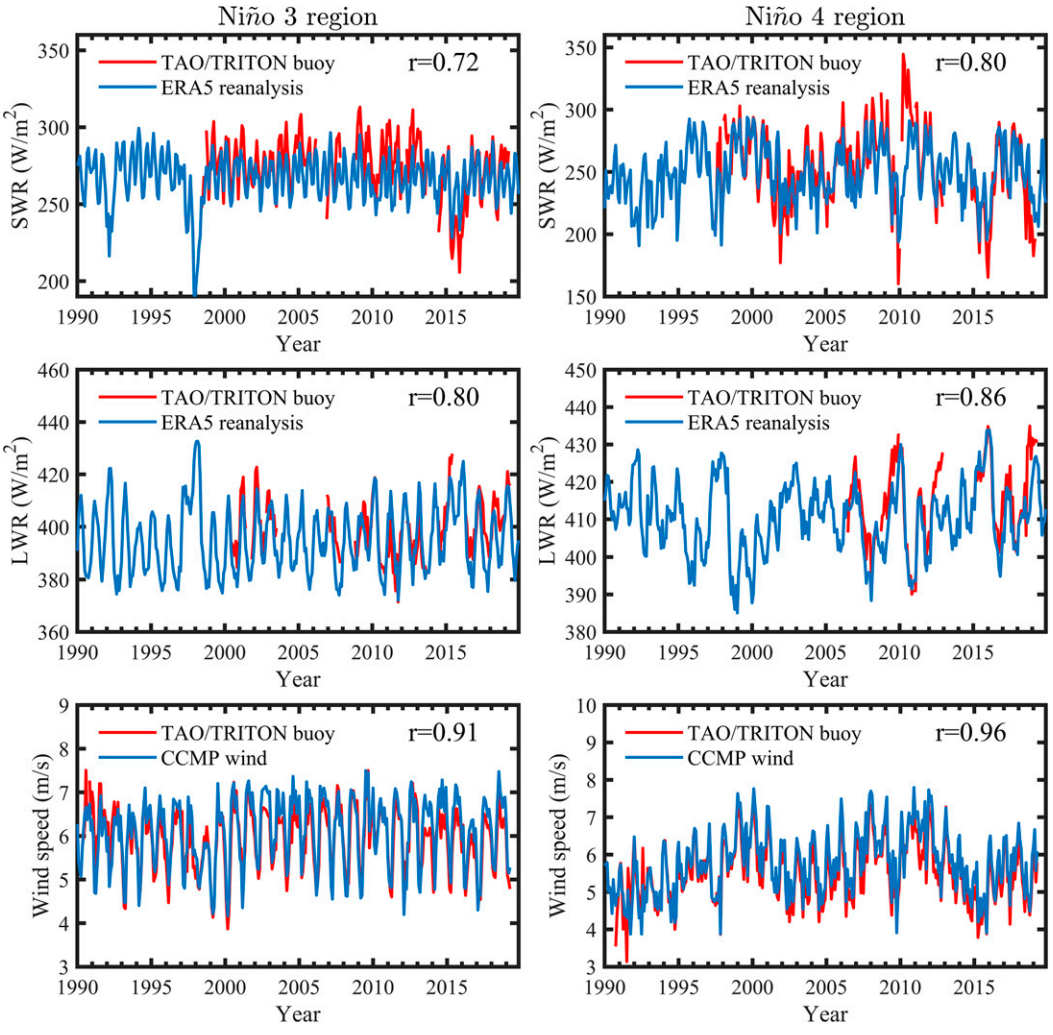

FIG. 3. Comparison of monthly mean (top) SWR, (middle) LWR, and (bottom) wind speed between the ERA5 reanalysis data, CCMP wind, and TAO/TRITON buoy observations in the (left) Niño-3 and (right) Niño-4 regions. The term *r* represents the corresponding correlation coefficient.

and satellite data, as well as in situ data from moored buoys, which could be more accurate than the reanalysis data. Then the gridded SWR, LWR, and wind data are linearly interpolated to the TAO/TRITON mooring locations. To be consistent with the TAO/TRITON array data, the period from 1990 to 2018 was selected. Figure 3 shows a comparison of SWR, LWR, and wind from the ERA5 data, CCMP data, and TAO/TRITON buoy observations. The correlation coefficients are all larger than 0.72 and could even reach 0.96. Thus, although the ERA5 reanalysis data and CCMP wind product contain uncertainties, the present variables are consistent with those in the TAO/TRITON array data in the Niño-3 and Niño-4 regions and can be used for further analysis.

b. Methods

To better understand ENSO diversity, several indices have been presented to identify different event types. In this study, the method in China National Standard GB/T 33666–2017 and Ren and Jin (2011) was used to identify EP and CP ENSO events and ENSO peak times (appendix A). Using this classification, both ENSO types are chosen for the period ranging from 1990 to 2018 (Table 1).

3. Results

a. Effects of two types of ENSO events on interannual variations in DSST in the Niño-3 and Niño-4 regions

To analyze the interannual variations, the DSST of each buoy is first averaged in each month. Monthly average DSST values greater than 1.5°C, although rare, could be seen in the Niño-3 region, while in the Niño-4 region DSST values larger than 1°C did not occur (Figs. 2b,c). The monthly DSST values are then averaged to produce a seasonal climatology, and the interannual DSSTA is obtained after subtracting the seasonal climatology from the monthly averaged time series. Once

TABLE 1. Classification of years based on the EP El Niño/La Niña and CP El Niño/La Niña phases and the related ENSO peak time during 1990–2018. The values in parentheses are the total number of DSSTs that are available (first and third numbers) and the probabilities of DSSTs that are larger than 0.5°C (second and fourth numbers, in italic font) during ENSO peak times in the Niño-3 region (set of numbers to the left of the semicolon) and 3-month lead ENSO peak times in the Niño-4 region (set of numbers to the right of the semicolon). The DSST values in both the Niño-3 and Niño-4 regions in 1991 and in 2007 in the Niño-3 region are not used in this paper because of the small quantity of data, and their probabilities are given as "NaN."

EP	CP
El Niño	
1991/92; Jan 1992 (844, *NaN*; 444, *NaN*)	1994/95; Dec 1994 (1748, *6.46%*; 1557, *15.80%*)
1997/98; Nov 1997 (1449, *12.63%*; 1527, *26.46%*)	2002/2003; Nov 2002 (1702, *5.64%*; 1608, *25.19%*)
2006/2007; Nov 2006 (1565, *7.35%*; 1493, *25.12%*)	2004/2005; Sep 2004 (1287, *5.91%*; 1656, *27.17%*)
2015/16; Dec 2015 (1060, *8.96%*; 1603, *22.83%*)	2009/10; Dec 2009 (1380, *8.62%*; 1802, *20.31%*)
	2018/19; Nov 2018 (1515, *4.16%*; 1164, *24.14%*)
La Niña	
1995/96, 1995.11 (1012, *24.31%*; 1528, *17.80%*)	2000/01, 2000.11 (1573, *16.97%*; 1475, *14.03%*)
1999/2000, 2000.01 (1711, *38.28%*; 1600, *7.88%*)	2011/12, 2011.12 (1185, *25.32%*; 1571, *7.00%*)
2007/08, 2008.01 (647, *NaN*; 1425, *6.95%*)	
2010/11, 2010.11 (1460, *26.51%*; 1656, *8.64%*)	
2017/18, 2018.01 (1443, *26.47%*; 1310, *10.31%*)	

completed DSSTA fields are created for the Niño-3 and Niño-4 regions (Fig. 2a), a time series of average fields is calculated to understand the mean DSSTA conditions and their relationships with the Niño SST indices, as shown in Fig. 1. The standard deviation of the DSSTA is approximately 0.09°C during this period in the Niño-3 region and is slightly larger than that in the Niño-4 region, which has a value of only 0.06°C. Moreover, as proposed above, the DSSTA in the Niño-3 region is negatively correlated with the Niño SST indices at a zero lag, while the DSSTA in the Niño-4 region is positively correlated with the Niño SST indices with a 3- to 4-month lead; it seems that the variation in the DSST could be regarded as an indicator of ENSO event occurrence. In this work, only the relationships between the DSSTA and the Niño SST indices are provided here; their interaction will be discussed in future research.

To further examine the interannual variations in DSST, the relationships between the DSSTA and Niño SST indices are identified for each ENSO year (Fig. 4). Because the DSSTA is negatively correlated with the Niño SST indices at a zero lag in the Niño-3 region, the mean values of the DSSTA during each EP/CP ENSO peak period (one month before and after peak times) are selected to study the interannual variation. Similarly, in the Niño-4 region, the DSSTA displays the mean values 3 months before the EP/CP ENSO peak periods because the DSST variation leads the Niño SST indices by 3 to 4 months. The classification standards for EP and CP ENSO events and the peak time corresponding to each event are shown in Table 1, and the values of the Niño SST indices and DSSTA are presented in Table 2. Note that because of the large-scale and long-term lack of measurements, the DSSTA data in 1991 in both the Niño-3 and Niño-4 regions and in 2007 in the Niño-3 region are not used in the following analysis.

As shown in Fig. 4a, during EP ENSO events, the DSSTA in the Niño-3 region generally decreases as the Niño-3 SST index increases. In EP El Niño events, the DSSTA values are all negative (i.e., smaller than −0.05°C; Table 2), whereas in EP La Niña events the DSSTA values are positive (i.e., larger than 0.05°C). The variation in DSST in the Niño-4 region is different from that in the Niño-3 region during EP ENSO events (Fig. 4b). When the Niño-3 SST index increases, the DSSTA in the Niño-4 region also increases. As shown in Table 2, during EP El Niño events, the DSSTA values are all positive in the Niño-4 region (i.e., larger than 0.04°C), but during EP La Niña events the DSSTA values are all negative (i.e., smaller than −0.02°C).

The variations in the DSST during the CP ENSO events are similar to those during EP ENSO events. The DSSTA in the Niño-3 region decreases as the Niño-4 SST index increases. Moreover, in CP El Niño events, the DSSTA values are all negative in the Niño-3 region (i.e., smaller than −0.09°C), whereas in CP La Niña events the DSSTA values are positive (i.e., larger than 0.03°C). In contrast, in the Niño-4 region, the DSSTA increases when the Niño-4 SST index increases. In addition, for CP El Niño events, the DSSTA values are all positive (i.e., larger than 0.02°C), whereas for CP La Niña events the DSSTA values are negative (i.e., smaller than −0.02°C).

The spatial and temporal averages of the DSSTA during different ENSO events in different regions, as shown above, may reduce the original extent of the DSST variation. Thus, the DSSTs of each buoy in the Niño-3 region and Niño-4 region are discussed to find the original variations in different ENSO events. Figure 5 shows the probability density functions (PDFs) and cumulative PDFs of the DSST in different ENSO events. The PDF distribution peaks appear at less than 0.3°C, and then the probabilities decrease as the DSST increases. The cumulative probabilities show that the small DSST in the Niño-3 region is greater in EP/CP El Niño years than in La Niña years but greater in EP/CP La Niña years than in El Niño years in the Niño-4 region. Here, we use 0.5°C as the criterion to separate large DSST and small DSST values. Basically, the probabilities of a large DSST are much larger in EP and CP La Niña years (more than 24.31% and 16.97%, respectively) than in EP/CP El Niño years (less than 12.63% and 8.62%) in the Niño-3 region (Table 1). In contrast, in the Niño-4 region, the probabilities of a large DSST are lower in EP and CP La Niña years (less than 17.80% and 14.03%, respectively) than in EP/CP El Niño years (more than 22.83% and 15.80%). As demonstrated in previous studies (Webster et al. 1996; Clayson and Bogdanoff 2013), the variation in the SST on the diurnal

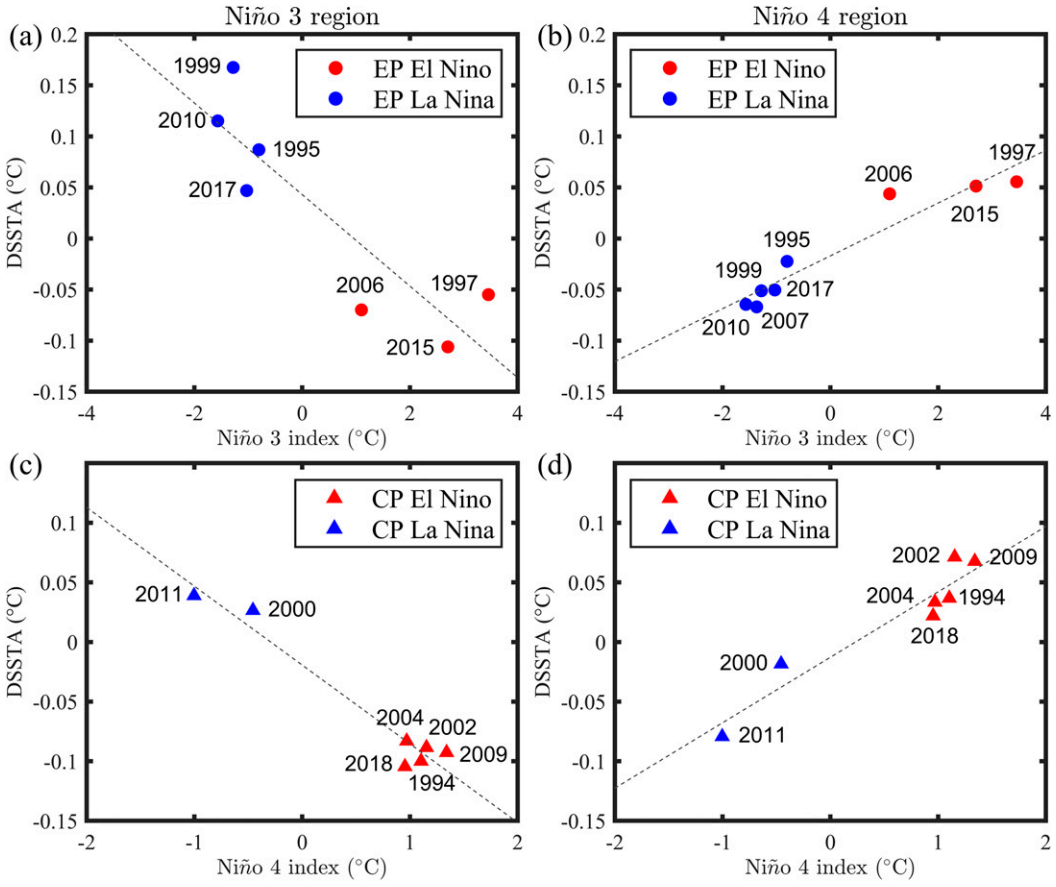

FIG. 4. Comparisons of the Niño SST indices and mean DSSTA during (a),(b) EP and (c),(d) CP (left) peak ENSO periods in the Niño-3 region and (right) 3-month-lead ENSO peak periods in the Niño-4 region. The El Niño and La Niña years are filled in red and blue, respectively.

time scale obviously impacts the tropical surface heat fluxes. Thus, the different probabilities of large DSST values in different ENSO events could also play an important role in the surface heat fluxes and further impact the evolution of different ENSO events; this topic requires further research through numerical experiments to explore the reverse effect of diurnal variation of SST on the evolution of different types of ENSO events.

TABLE 2. Niño SST indices and DSSTA in different types of ENSO events in the Niño-3 and Niño-4 regions.

EP ENSO						CP ENSO					
El Niño			La Niña			El Niño			La Niña		
Year	SSTA	DSSTA	Year	SSTA	DSSTA	Year	SSTA	DSSTA	Year	SSTA	DSSTA
					Niño-3 region						
1997	3.46	−0.05	1995	−0.80	0.08	1994	1.10	−0.10	2000	−0.46	0.03
2006	1.10	−0.07	1999	−1.30	0.17	2002	1.15	−0.09	2011	−1.00	0.04
2015	2.70	−0.11	2010	−1.70	0.11	2004	0.97	−0.09			
			2017	−1.03	0.05	2009	1.34	−0.09			
						2018	0.95	−0.10			
					Niño-4 region						
1997	3.46	0.06	1995	−0.80	−0.02	1994	1.10	0.04	2000	−0.46	−0.02
2006	1.10	0.04	1999	−1.30	−0.05	2002	1.15	0.07	2011	−1.00	−0.08
2015	2.70	0.05	2007	−1.37	−0.07	2004	0.97	0.03			
			2010	−1.70	−0.06	2009	1.34	0.07			
			2017	−1.03	−0.05	2018	0.95	0.02			

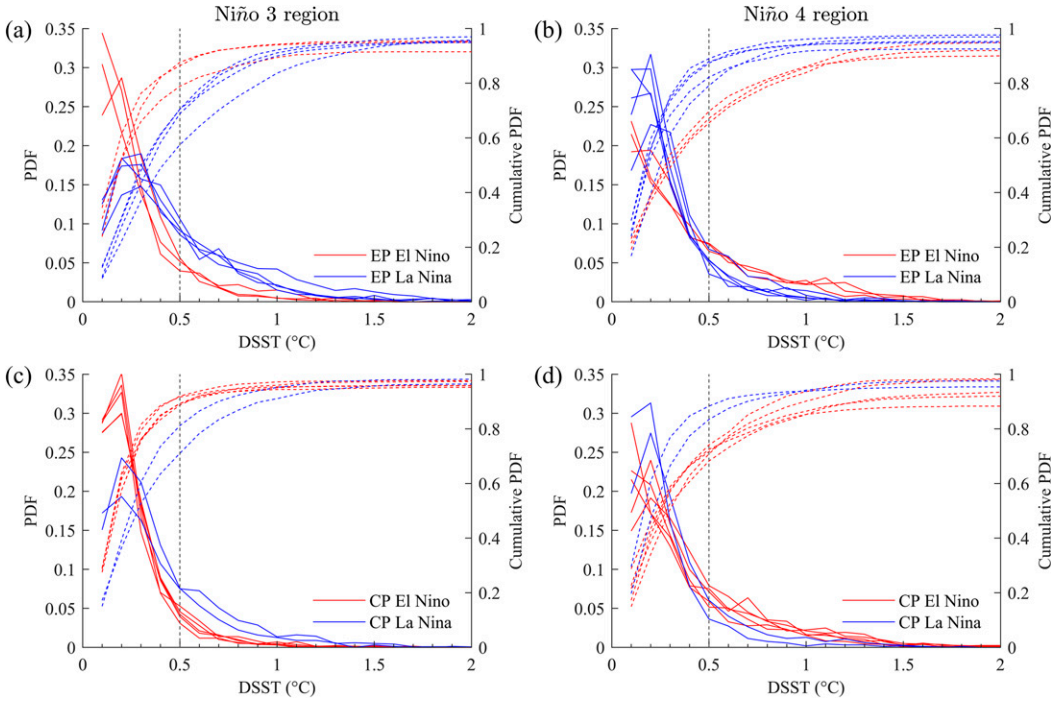

FIG. 5. PDFs (solid lines) and cumulative PDFs (dashed lines) of the DSST in (a),(b) EP and (c),(d) CP ENSO events in the (left) Niño-3 and (right) Niño-4 regions. The black vertical dashed lines represent the location of 0.5°C.

Based on the above analysis, it is clear that the DSSTs in the Niño-3 and Niño-4 regions show different interannual variations and have different relationships with the Niño SST indices. These results highlight the different physics at work on these two types of ENSO events. Next, we will explain these differences by comparing climate conditions, including SWR, wind, LWR, SHF, and LHF variations, during the two types of ENSO events.

b. *Causes of interannual variation in DSST during different types of ENSO events*

Based on previous studies, SWR and wind are the dominant processes controlling the variations in DSST (Webster et al. 1996; Gentemann et al. 2008; Yang et al. 2015). Strong SWR and calm conditions will lead to a large DSST, whereas weak SWR and strong wind will cause the diurnal variation to be imperceptible (Kawai and Wada 2007). However, the effect of wind could be captured not only in wind stress (WS) but also in LHF. Then whether WS or LHF plays a more important role in influencing the DSST needs to be investigated. Moreover, other factors, such as LWR and SHF, may also affect the diurnal variations during the two types of ENSO events. To determine the effective factors that influence the interannual variation in DSST among SWR, WS, LWR, SHF, and LHF, a parameterization formula for DSST estimation is first developed based on Fairall et al. (1996a). The detailed process of the formula is explained in appendix B. Note that the variation of temperature due to ocean dynamics, such as horizontal advection and entrainment, could not be recognized well in this parameterized model, similar to other mixed-layer models. This may be the reason for the damped amplitude of the simulated DSSTA in the Niño-3 region relative to that in the Niño-4 region. However, the overall interannual variations in the parameterized results show good agreements with the observed DSSTs, and the correlation coefficients could reach 0.73 and 0.82 in the Niño-3 region and Niño-4 region, respectively. This provides support for the hypothesis that the parameterization formula is reliable and can be used to perform further sensitivity experiments, which will help us uncover the specific processes that lead to the interannual variation in the DSST.

To reveal the relative roles of each forcing factor, namely SWR, WS, LWR, SHF (upward), and LHF (upward), in inducing the interannual variation in the DSST, we design six experiments, which include one control run and five sensitivity runs. The control run is forced by surface heat fluxes and WS all with interannual variations, which is the same as the experiment shown in appendix B. For the sensitivity runs, we specify one of the five forcing fields with a climatological variation. Therefore the difference between the control run and the sensitivity runs could be treated as the contribution of the interannual variation in the specific forcing fields (Fig. 6). The details of the forcing conditions for each of the sensitivity experiments are shown in Table 3. Note that the effect of precipitation, which may also impact the DSST to some extent, is not considered in this study. One reason is that the warm-layer model of Fairall et al. (1996a) we referred to does not include the effect of precipitation. The other reason is that according to Webster et al. (1996), the dependence of diurnal warming on

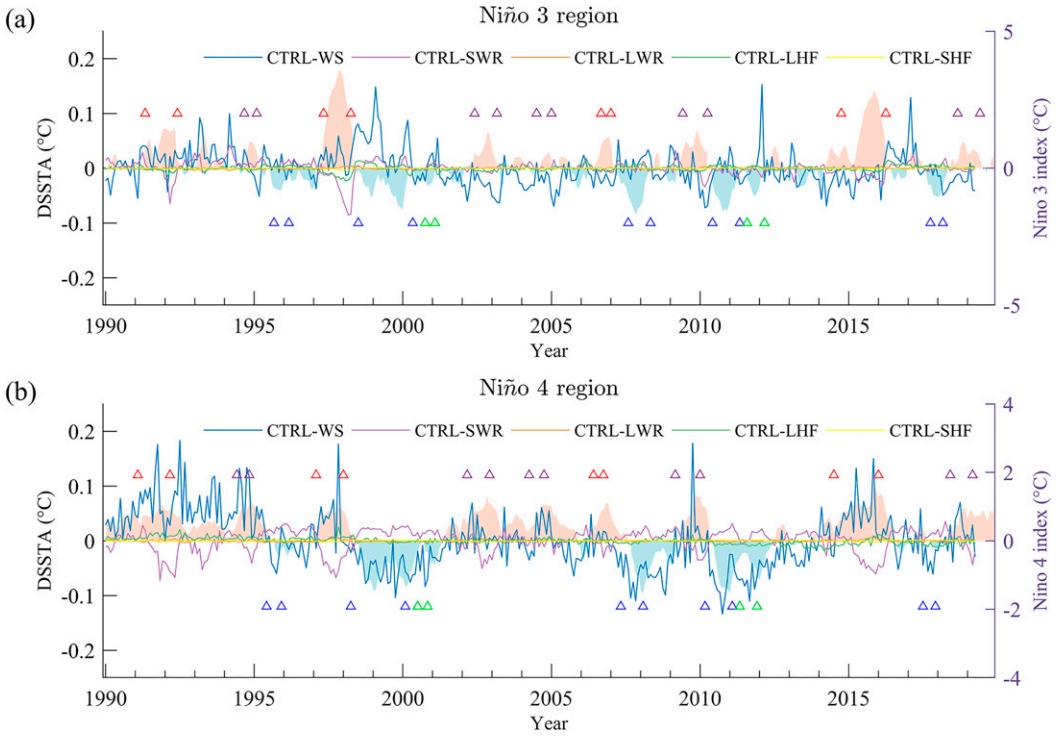

FIG. 6. Differences of DSSTA between that in control experiment and those in sensitivity experiments in the (a) Niño-3 and (b) Niño-4 regions. The shaded plots are the Niño indices. The triangles represent the start and stop time of each ENSO event (red: EP El Niño, purple: CP El Niño, blue: EP La Niña, green: CP La Niña).

precipitation is much smaller than that on SWR and wind speed, and the effect is most influential under high precipitation inputs and weak winds, which does not occur frequently. The importance of precipitation will be discussed in future work.

Figure 6 presents the differences of the DSSTA between the results simulated in the control run and those in each of the sensitivity experiments from January 1990 to December 2018. When the difference is near zero, the result in the sensitivity experiment is similar to that in the control run. Then the specific forcing factor has an insignificant contribution to the interannual variation in DSST. The larger the difference leaves zero, the more influence the factor has. Besides, when the difference is positive, it illustrates that the factor will increase the DSST; while when the difference is negative, the factor will reduce the DSST. As shown in the figure, the WS and SWR have much more significant impacts than LWR, SHF, and LHF have on the interannual variation in DSST, especially in the Niño-4 region. When compared with Niño indices, the SWR always causes DSST to decrease during El Niño and increase during La Niña in both the Niño-3 and Niño-4 regions. However, the effects of WS on DSST are opposite in the two regions. In the Niño-3 region, the WS always causes DSST to decrease during El Niño and increase during La Niña, but in the Niño-4 region the WS turns to increase the DSST during El Niño and decrease during La Niña. The reason will be discussed in the following.

To quantitatively assess the contributions from each of the five factors, we calculate the actual change in the DSST range and the percentage change contributed by each factor in different ENSO types in the Niño-3 and Niño-4 regions according to Yang et al. (2015). The percentage change is defined as the ratio of the actual change in DSST relative to the total change of the five sensitivity experiments. The percentage change results are shown in Fig. 7.

In the Niño-3 region, the factors that influence the variations in DSST are complex and are different in EP ENSO and CP ENSO (Figs. 7a,c). In EP ENSO, the dominant role is the SWR, which accounts for 47.1% of the total changes. In addition, the LHF also contributes to 32.4% of the changes, while the WS accounts for 18.6% of the changes. Other factors, including LWR and SHF (−2.3% and 4.3%, respectively), do not exert a great influence. During CP ENSO, the WS (74.3%)

TABLE 3. List of all sensitivity runs in this study, giving the forcings for the different kinds of surface fluxes. Here "I" represents the forcing with the interannual variation and "C" represents the climatology forcing without the interannual variation.

Expt	SWR	WS	LWR	LHF	SHF
CTRL	I	I	I	I	I
EXP_SWR	C	I	I	I	I
EXP_WS	I	C	I	I	I
EXP_LWR	I	I	C	I	I
EXP_LHF	I	I	I	C	I
EXP_SHF	I	I	I	I	C

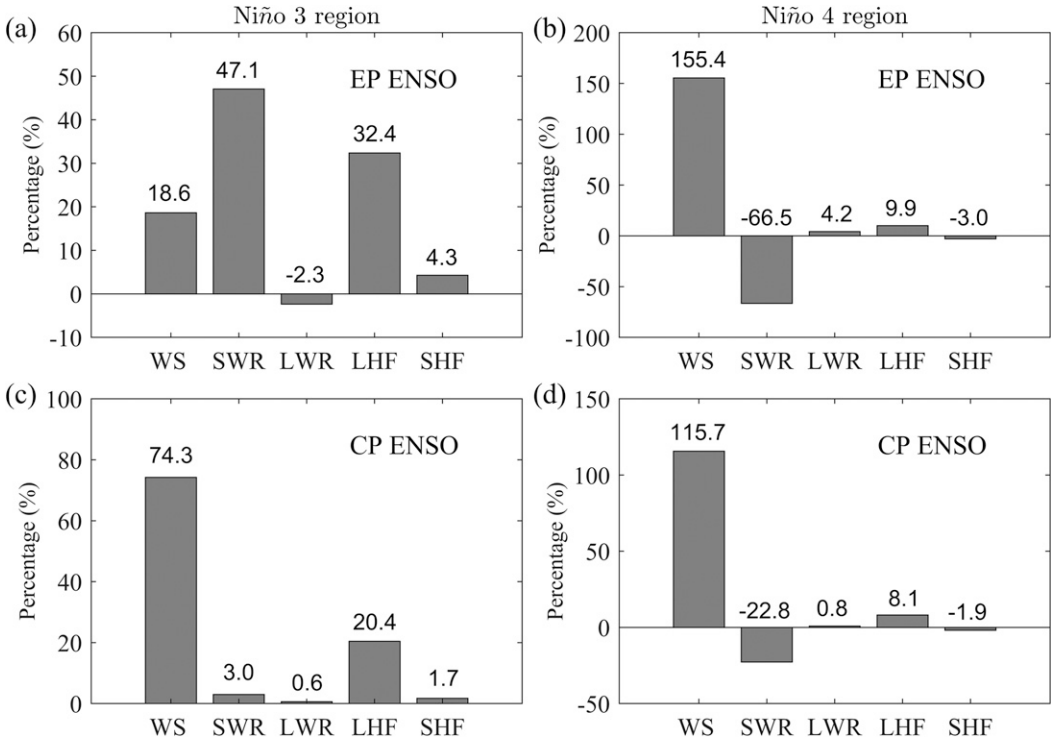

FIG. 7. The contributions of each surface forcing factor in the (left) Niño-3 and (right) Niño-4 regions during (a),(b) EP and (c),(d) CP ENSO events.

plays a key role in the ENSO periods, while the second most effective factor is the LHF, which accounts for 20.4%. Other factors, such as the SWR (3.0%), LWR (0.6%), and SHF (1.7%), only have weak effects.

In the Niño-4 region, the factors that impact the interannual variation in DSST exhibit some similarities in EP ENSO and CP ENSO (Figs. 7b,d). In both two types of ENSO, WS is the dominant factor, and the ratios could reach 155.4% and 115.7%, respectively. However, the SWR causes inverse effects in the interannual variation in the DSST, which has ratios of −66.5% and −22.8%, respectively. The inverse effects imply that the SWR may reduce the amplitude of the interannual variation. Other factors, including LWR (4.2% and −0.8%, respectively), LHF (9.9% and 8.1%, respectively), and SHF (−3.0% and −1.9%, respectively), have much smaller effects.

In conclusion, WS plays the dominant role in influencing the interannual variation in the DSST most of the time, except during EP ENSO in the Niño-3 region, which has the SWR as the key factor. In the Niño-3 region, the LHF acts as the second most important factor during both types of ENSO, while it is insignificant in the Niño-4 region. This may occur due to the obvious interannual variation in the LHF in the Niño-3 region and the nonsignificant interannual variation in the Niño-4 region (Fig. 8). Excluding the positive effects, some factors play negative roles in affecting the DSST, such as the SWR in the Niño-4 region during both types of ENSO.

To determine how the atmospheric factors influence the interannual variation in the DSST, the WS, SWR, and LHF during different ENSO types in different regions are shown in Fig. 8, since those three factors play more important roles than other factors. In general, the SWR is weaker during El Niño events than that during La Niña events in both the Niño-3 region and Niño-4 region. After comparing the variation in SWR with the variation in total cloud cover, the parameters both show notable negative correlations (−0.88 and −0.86 in the Niño-3 and Niño-4 region, respectively), which can be explained by Eq. (3) in Reed (1977) that reveals the relation between SWR and cloud cover. The results imply that the decreased incidence of SWR into the ocean is entirely caused by the increased total cloud cover during El Niño and that the increased incidence of SWR into the ocean is entirely caused by the decreased total cloud cover during La Niña. However, the SWR in the Niño-3 region during CP La Niña is not obviously stronger than that during CP El Niño (Fig. 8c). This may occur due to the spatial limitation of CP ENSO (Capotondi et al. 2015), which will hardly impact the mean SST and total cloud coverage in the Niño-3 region.

The WS in the Niño-4 region decreases during both types of El Niño events but increases during both types of La Niña events. The WS in this region varies mainly due to the trade wind, which is directly caused by SST differences between the western Pacific and EP. During El Niño events, there is an obviously weakened trade wind due to the decrease in the SST difference between the western Pacific and EP, which could further create a positive SSTA in the EP; this positive feedback is well known as Bjerknes feedback (Bjerknes 1969). Similarly, during La Niña, the strength of the trade wind is obviously enhanced by the increased SST difference. Note that the

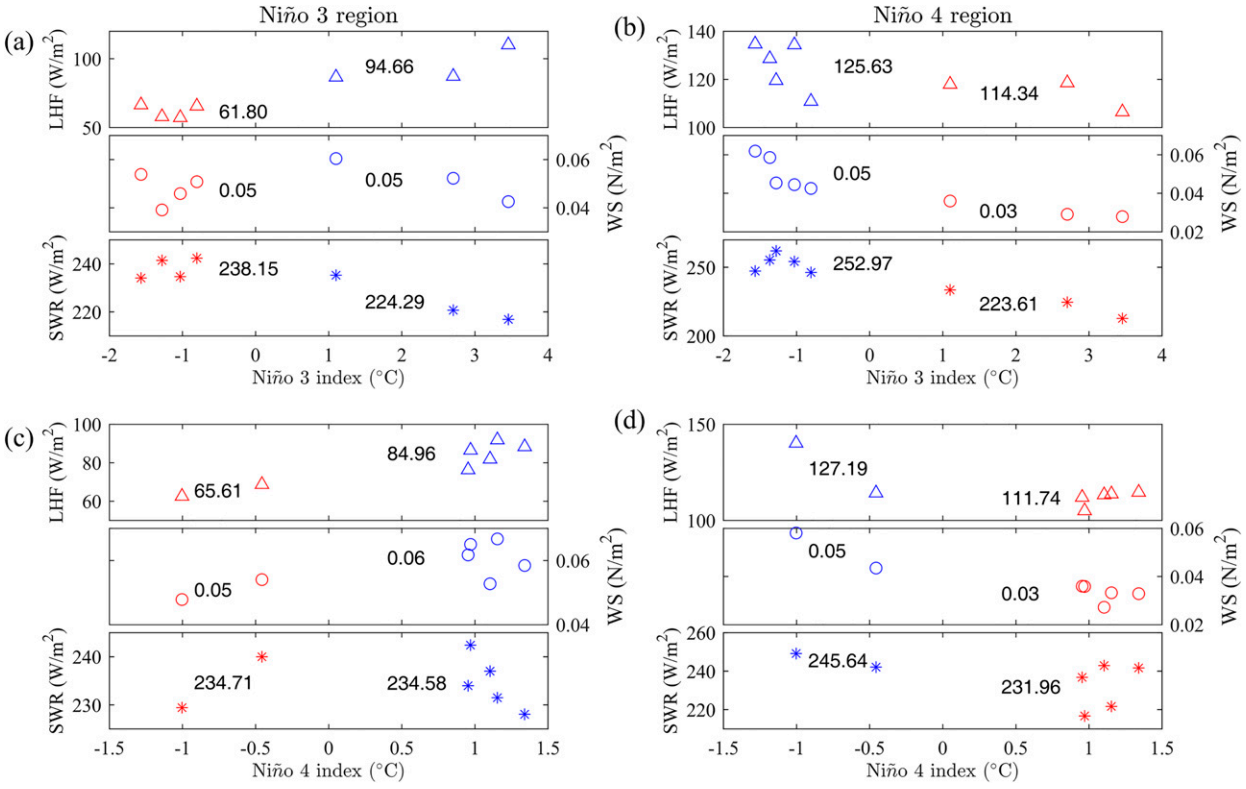

FIG. 8. Comparisons of the Niño SST indices and SWR (asterisks), WS (circles), and LHF (triangles) during (a),(b) EP and (c),(d) CP (left) ENSO peak periods in the Niño-3 region and (right) 3-month-lead ENSO peak periods in the Niño-4 region. The mean values of these forcing factors during those periods are also given in the plots. The color represents whether the DSSTA is positive (red) or negative (blue) during this period.

DSSTA in the Niño-4 region leads the Niño SST indices by 3–4 months, which is mainly because the westerly wind bursts precede the occurrence of ENSO events by one or several months, as has been reported by Feng et al. (2020) and Wang et al. (2019). In the Niño-3 region, the WS behaves moderately and irregularly during the EP ENSO events, but the reason for this phenomenon has not yet been identified. During CP ENSO events, the WS during El Niño is larger than that during La Niña, in contrast with that in the Niño-4 region. This variation may be due to the two-cell circulation generated by the upward flow over the warm SST in the CP in an evolving El Niño, which results in the easterly flow to the east of the convection and the two-cell circulation generated by the downward flow over the cold SST in the CP in an evolving La Niña, which results in the westerly flow to the east of the convection (Sarachik and Cane 2010).

The LHF in the Niño-3 region shows obvious interannual variation, which increases during El Niño and decreases during La Niña in both types of ENSO events. After comparing the heat fluxes, we find that the interannual variation in the LHF is more obvious and stronger than that in the LWR and SHF (figure not shown), which explains why the LWR and SHF have insignificant effects in all cases. In the Niño-4 region, the LHF also shows an interannual variation to some extent, but the variation is not as large as and contrasts to that in the Niño-3 region (i.e., decreased during El Niño and increased during La Niña). The reason may be that the LHF is intrinsically related to the wind and SST. The increased SSTs during the El Niño events will lead to the consequent enhanced vertical moisture gradient between the surface and overlying air, which will increase the LHF. Conversely, the decreased SSTs during the La Niña events will lead to the consequent reduced vertical moisture gradient between the surface and overlying air, which will decrease the LHF. In addition, the strengthened or weakened WS in the Niño-3 region during the CP ENSO events will also result in increased or decreased LHF, respectively. Thus, the interannual variation of LHF in the Niño-3 region becomes obvious. However, in the Niño-4 region, the reduced WS during El Niño will lead to decreased LHF and conversely the enhanced WS during La Niña will lead to increased LHF. The combined effect of SST and WS results in the reduced interannual variation in the Niño-4 region (Figs. 8b,d). Moreover, under the influence of the WS with significant interannual variation, the LHF with weak interannual variation plays an inconspicuous role in influencing the DSSTA in the Niño-4 region.

c. *Mechanism analysis*

This study suggests that the interannual variations in DSST are caused mainly by different WS, SWR, and LHF behaviors

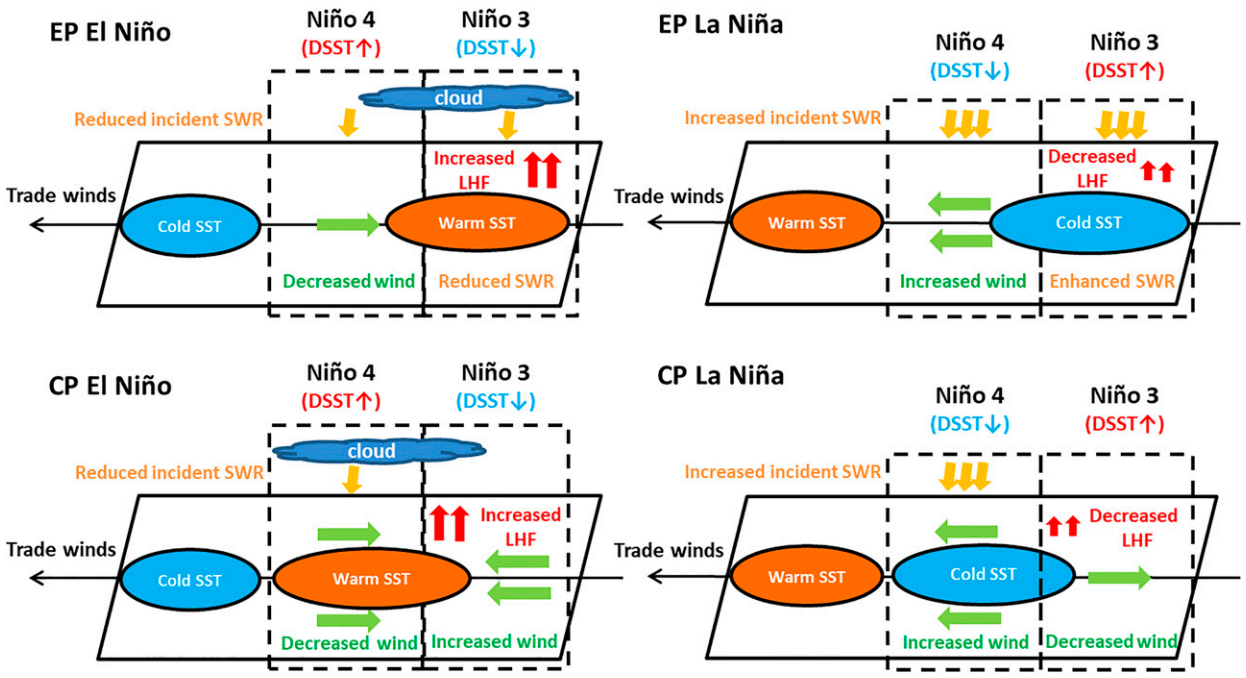

FIG. 9. Schematic of the mechanisms of different El Niño and La Niña types in the interannual variations in DSST. In the Niño-3 region during EP El Niño, the warm SST will lead to large total cloud cover due to enhanced convection, which further reduces the incident SWR, and also the upward LHF increases. In the Niño-3 region during EP La Niña, the cold SST will lead to small total cloud cover due to reduced convection, which further enhances the incident SWR, and also the upward LHF decreases. With the combined effects of incident SWR and LHF, the DSST decreased and increased during EP El Niño and La Niña, respectively. During the CP El Niño, the WS was enhanced by the two-cell circulation generated by the upward flow over the warm SST in the CP in an evolving El Niño, and moreover the upward LHF increased. During the CP La Niña, the WS was weakened by the two-cell circulation generated by the downward flow over the cold SST in the CP in an evolving La Niña, and moreover the upward LHF decreased. Both the WS and LHF will contribute to decreased and increased DSST during CP El Niño and La Niña events, respectively. In the Niño-4 region, the trade wind decreases during EP and CP El Niño events and increases during EP and CP La Niña events because of the Bjerknes feedback. The variation in WS will lead to increases in DSST during EP and CP El Niño events and decreases in DSST during EP and CP La Niña events. However, the reduced and enhanced incident SWR respectively related to the large and small total cloud cover will weaken the extent of DSST variation.

during different types of ENSO events. Next, we are trying to explore the physical process of how the surface atmospheric forcing factors regulate the interannual variation in the DSST. Based on the above analysis, the mechanisms can be summarized as follows (Fig. 9): in the Niño-4 region, approximately 3 months before both EP and CP El Niño events, the wind speed starts to decrease with the weak trade wind. At the same time, the total cloud cover tends to increase because of the warming of the SST, which further contributes to the decrease in the incident SWR. The decreased wind leads to a large DSST in this region. However, the reduced SWR weakens the extent of DSST variation, but the effects are not as strong as those of the WS. Conversely, in that same region, approximately 3 months before both EP and CP La Niña events, the wind speed starts to increase with the strong trade wind. At the same time, the total cloud cover tends to decrease due to the cooling of the SST, which further contributes to the increase in the incident SWR. The increased wind leads to a small DSST in this region. However, the enhanced SWR weakens the extent of DSST variation, but the effects are again not as strong as those of the WS.

In the Niño-3 region during EP El Niño, the warm SST leads to an increase in total cloud cover by enhancing convection, which results in a weak incident SWR. Moreover, the upward LHF increased obviously. The combined effect of SWR and LHF generates a small DSST. Conversely, in that same region during EP La Niña, the cold SST leads to a decrease in total cloud cover by reducing convection, which results in a strong incident SWR. Moreover, the upward LHF decreased obviously. The combined effect of SWR and LHF generates a large DSST. Simultaneously, the moderate wind speeds during the period also impact the variation in the DSST to a certain extent.

During CP El Niño and La Niña in the Niño-3 region, the winds respectively increased and decreased as a result of the two-cell circulation discussed above. In addition, the upward LHF was also enhanced during El Niño and reduced during La Niña. The combination of the two factors, especially the effect of WS, leads to obviously low diurnal warming during El Niño and high diurnal warming during La Niña. However, the irregularly varied SWR does not have an effective effect on the DSST in this case.

Taking all of the above into consideration, the interannual variation in DSST in the Niño-3 region is controlled by both the variation in the SWR (in EP ENSO), WS (in CP ENSO),

and the LHF (in both EP and CP ENSO). However, the interannual variation in the Niño-4 region is mainly dominated by the variation in WS in both EP and CP ENSO events. The opposing effects of the incident SWR to the DSST in the Niño-4 region may reduce the amplitude of its interannual variation.

4. Discussion and conclusions

The variation in the diurnal SST in the tropical Pacific Ocean is important because of its nonnegligible effects on air–sea interactions. The interannual variations in DSST under different types of ENSO were examined using long-term observations, and the influencing mechanisms were discussed in this paper.

First, we found different interannual DSST variations in the Niño-3 and Niño-4 regions. The DSSTA in the Niño-3 region was negatively correlated with the Niño-3 SST index (correlation coefficient: −0.57) and Niño-4 SST index (correlation coefficient: −0.69) with zero lag, while in the Niño-4 region the DSSTA was positively correlated with the Niño-3 SST index (correlation coefficient: 0.44) and Niño-4 SST index (correlation coefficient: 0.55) with a 3- to 4-month lead. In addition, in the Niño-3 region, the probabilities of a large DSST (>0.5°C) were significantly lower in EP and CP El Niño years (less than 12.63% and 8.62% respectively) than in the EP and CP La Niña years (more than 24.31% and 16.97% respectively). In contrast, in the Niño-4 region, the probabilities were obviously higher in the EP and CP El Niño years (more than 22.83% and 15.80% respectively) than in the EP and CP La Niña years (less than 17.80% and 14.03% respectively).

By analyzing the relationships among the DSSTA and surface forcing factors during ENSO periods, this study identified that the SWR, WS, and LHF were different factors causing the different interannual variations in DSST in the Niño-3 region and Niño-4 region, respectively. In the Niño-3 region, the SWR (in EP ENSO events) and WS (in CP ENSO events) were the main reasons for the variation in DSST. In addition, the LHF also effectively impacts the DSST variation in both EP and CP ENSO events. In the Niño-4 region, the WS was the dominant factor influencing the DSST in both EP and CP ENSO events. In addition, the relatively low or high SWRs during El Niño or La Niña, respectively, decrease the extent of interannual variation in DSST in the Niño-4 region. Note that the contribution of ocean dynamics, which is also important in SST variation during ENSO events (McPhaden 1999, 2004), is ignored in this study due to the limitation of the parameterization model and needs to be pursued for completeness in future work. To adequately access the impacts of ocean dynamics on the interannual variation in DSST, a three-dimensional model containing the exact ocean processes is necessary.

Because the tropical Pacific Ocean and atmosphere are coupled, the diurnal variation in SST may generate further changes in the SST climatology and variability, through air–sea interactions (Danabasoglu et al. 2006; Bernie et al. 2008; Tian et al. 2019). The impacts on the interannual variation in SST (i.e., ENSO events) have attracted increasing attention in previous studies (Danabasoglu et al. 2006; Ham et al. 2010; Masson et al. 2012; Tian et al. 2019). However, they focused mainly on the effect of the DSST on ''canonical'' ENSO events (i.e., EP ENSO or ENSO defined using the Niño-3.4 index) while rarely paying attention to CP ENSO events. Using a one-dimensional mixing model, Wu (2013) noted that the large DSST that occurred before the CP El Niño event in 2009 would have contributed to a warmer SST in the following month due to reduced mixing at the base of the mixed layer and the suppression of entrainment, which verifies the effect of DSST on the evolution of the CP ENSO. In fact, with the increasing frequency and persistent occurrence of CP El Niño events (Lee and McPhaden 2010), large diurnal warming in the central equatorial Pacific would occur more frequently, which may further influence the mean SST and change the frequency of CP ENSO events in the future. Further investigations are required to clarify these issues using coupled models.

Acknowledgments. We acknowledge the three anonymous reviewers and the editor, Dr. Benjamin Richard Lintner, for their constructive comments and suggestions for improving the paper. This work is supported by the National Key R&D Program of China (Grants 2017YFC1404000), the National Natural Science Foundation of China (Grants 41906029, 42022042, and 41821004), the China–Korea Northwestern Pacific Climate Change and Its Prediction cooperation project, and the CAS Interdisciplinary Innovation Team (JCTD-2020-12).

Data availability statement. The TAO/TRITON data used in this study are available at https://www.pmel.noaa.gov/tao/drupal/disdel/. The SWR and LWR data from ERA5 reanalysis data and the wind data from the Cross-Calibrated Multi-Platform (CCMP) are available at https://cds.climate.copernicus.eu/cdsapp#!/dataset/reanalysis-era5-single-levels-monthly-means?tab=form and http://data.remss.com/ccmp/, respectively. The scripts used in the analysis and other supporting information useful to reproduce the authors' work can be obtained by contacting the corresponding author.

APPENDIX A

ENSO Types [China National Standard GB/T 33666–2017 and Ren and Jin (2011)]

Before dividing ENSO events into different types, the ENSO events need to be identified. First, the Niño-3.4 SST index is calculated over the Niño-3.4 region (5°N–5°S, 170°–120°W) using the time series of the Hadley Centre SST dataset (HadISST) from 1950 to 1981 and the NOAA ¼° daily Optimum Interpolation Sea Surface Temperature (OISST v2) from 1982 to 2019 by removing the seasonal climatology. Note that the 30-yr moving climate state recommended by the World Meteorological Organization is adopted to calculate the seasonal climatology, which means that the Niño index from 1950 to 1990 is calculated by subtracting the seasonal climatology between 1951 and 1980, whereas the Niño index from 1991 to 2000 is calculated by subtracting the seasonal climatology between 1961 and 1990. Then, an El Niño year is defined as a year in which the 3-month running mean Niño-3.4 index is greater than 0.5°C and lasts at least 5 months and a La Niña year is defined as a year in which the 3-month running mean Niño-3.4 index is less than −0.5°C and lasts at least 5 months. Moreover,

the peak time is defined as when the Niño-3.4 index reaches its maximum value during each ENSO event.

Second, the EP ENSO index [Eq. (A1)] and CP ENSO index [Eq. (A2)] are calculated using the Niño-3 SST index and Niño-4 SST index, which are calculated over the Niño-3 region and Niño-4 region, respectively, in the same way as the Niño-3.4 SST index:

$$I_{\mathrm{EP}} = I_{\mathrm{NINO3}} - \alpha I_{\mathrm{NINO4}} \quad \text{and} \tag{A1}$$

$$I_{\mathrm{CP}} = I_{\mathrm{NINO4}} - \alpha I_{\mathrm{NINO3}}, \tag{A2}$$

where I_{EP} is the EP ENSO index, and I_{CP} is the CP ENSO index. When $I_{\mathrm{NINO3}} \times I_{\mathrm{NINO4}} > 0$, $\alpha = 0.4$; when $I_{\mathrm{NINO3}} \times I_{\mathrm{NINO4}} \le 0$, $\alpha = 0$.

An ENSO event is classified as an EP or CP type when the absolute value of I_{EP} or I_{CP}, respectively, exceeds 0.5 and lasts for at least 3 months. The ENSO events and ENSO types pronounced using this method from 1990 to 2018 are shown in Table A1.

TABLE A1. El Niño/La Niña events from 1990 to 2018.

Period	Peak time	Type
El Niño		
May 1991–Jun 1992	Jan 1992	EP
Sep 1994–Feb 1995	Dec 1994	CP
May 1997–Apr 1998	Nov 1997	EP
Jun 2002–Mar 2003	Nov 2002	CP
Jul 2004–Jan 2005	Sep 2004	CP
Sep 2006–Jan 2007	Nov 2006	EP
Jun 2009–Apr 2010	Dec 2009	CP
Oct 2014–Apr 2016	Dec 2015	EP
Sep 2018–Jun 2019	Nov 2018	CP
La Niña		
Sep 1995–Mar 1996	Nov 1995	EP
Jul 1998–May 2000	Jan 2000	EP
Oct 2000–Feb 2001	Nov 2000	CP
Aug 2007–May 2008	Jan 2008	EP
Jun 2010–May 2011	Nov 2010	EP
Aug 2011–Mar 2012	Dec 2011	CP
Oct 2017–Mar 2018	Jan 2018	EP

APPENDIX B

Diurnal Warming Estimation

To estimate the diurnal warming in SST, we refer to the warm-layer model proposed by Fairall et al. (1996a). According to Fairall et al. (1996a), the warm layer will be established quickly when the instantaneous solar radiation absorbed above the warm layer exceeds the nonsolar radiation fluxes, and thus the variation in the near-surface temperature and current will be induced by the temporal integrals of the heat fluxes and momentum fluxes, respectively, as follows:

$$\Delta T_w = \frac{2\int(\delta S_w - Q)\,dt}{\rho c_p D_T} = \frac{2I_s}{\rho c_p D_T} \quad \text{and} \tag{B1}$$

$$\Delta u_w = \frac{2\int\frac{\tau}{\rho}dt}{D_T} = \frac{2I_\tau}{D_T}, \tag{B2}$$

where ΔT_w denotes the temperature change between the surface and reference depth (without diurnal variation); δS_w is the instantaneous solar radiation in the warm layer; Q represents the nonsolar radiation fluxes consisting of the LWR, SHF, and LHF; ρ is the seawater density; c_p is the volumetric heat capacity; I_s is the integral of heat fluxes; D_T is the warm layer depth; u represents the magnitude of the current; τ is the wind stress, and I_τ is the integral of momentum fluxes. Note that the COARE 2.6 bulk flux parameterization developed by Fairall et al. (1996b) is used to compute the SHF, LHF, and wind stress using atmospheric data.

The value of D_T can be obtained by requiring the bulk Richardson number to be no greater than a critical value, which is 0.65 in this study:

$$D_T = \left(\frac{2\rho c_p \mathrm{Ri}_c}{\alpha g I_s}\right)^{1/2} I_\tau, \tag{B3}$$

where α is the thermal expansion coefficient and g is the gravity acceleration.

According to Eqs. (B2) and (B3), Eq. (B1) can be transformed into the following equation:

$$\Delta T_w = \frac{I_s^{3/2}}{I_\tau} \times \mathrm{const} = \frac{\left[\int(\delta S_w - Q)\,dt\right]^{3/2}}{\int\frac{\tau}{\rho}dt} \times \mathrm{const}\,, \tag{B4}$$

where

$$\mathrm{const} = \frac{2(\alpha g)^{1/2}}{(2\mathrm{Ri}_c)^{1/2}(\rho C_p)^{3/2}}.$$

It has been shown that ΔT_w represents the temperature change between the surface and reference depth [a depth without diurnal warming; 19 m in Fairall et al. (1996a)]. As no solar heat fluxes reach the surface during the nighttime, the upper layer will be well mixed by turbulence and convection. Then, we treat $\Delta T_{w\text{-night}}$ as being equal to zero. During the daytime, the absorption of solar radiation contributes to building a stable stratified warm layer, and the SST starts to increase. The SST will reach a daily maximum when the sun goes down, and the solar radiation achieves a balance with the nonsolar radiation fluxes. At this time, $\Delta T_{w\text{-day}}$ can be regarded as ΔT_w. Then, $\Delta T_{w\text{-day}}$ is calculated as discussed below.

a. Calculation of I_s.

First, the daily mean solar radiation is reconstructed for the diurnal cycle, which is proportional to $\cos[(\pi/2)(t - 12)/6]$ between 0600 and 1800 local time (LT) in reference to Filipiak et al. (2012) and is set to zero at other times. Then, the nonsolar fluxes (including net LWR, SHF, and LHF) are calculated based on the bulk formulas developed by Fairall et al. (1996b)

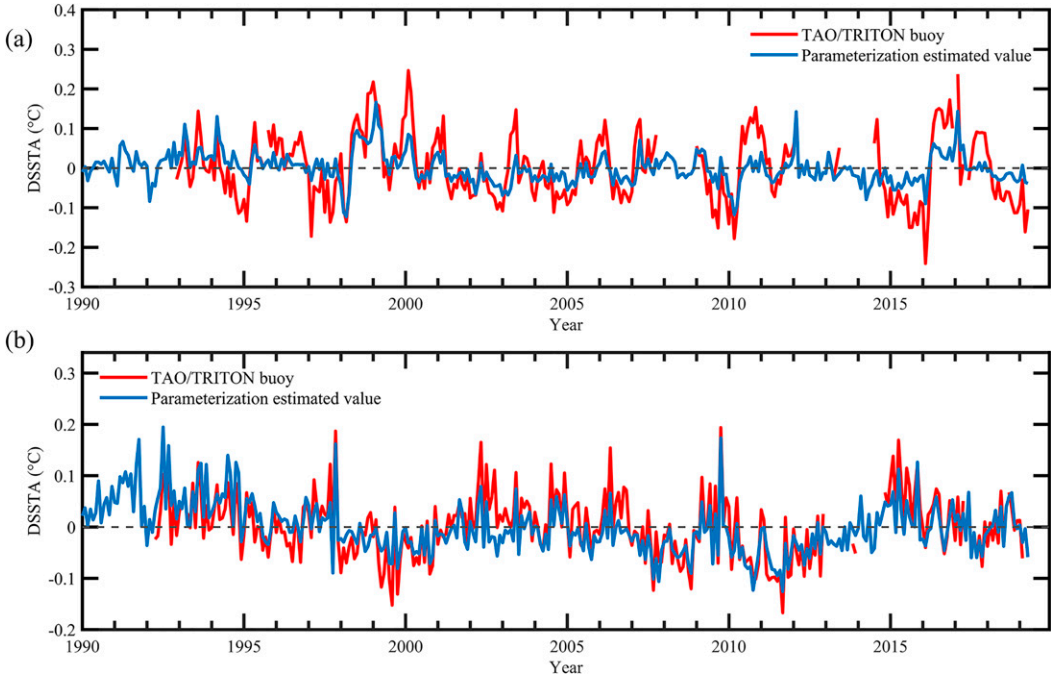

FIG. B1. Comparison of DSSTA from TAO/TRITON buoy observations and that estimated using the parameterization method in the (a) Niño-3 and (b) Niño-4 regions.

using atmospheric inputs such as air temperature, specific humidity, and air pressure, from ERA5 reanalysis data and the wind speed from CCMP data. The term I_s is the integral of heat fluxes when the instantaneous solar radiation starts to exceed the nonsolar radiation fluxes to the time when the SST reaches a daily maximum (i.e., the solar radiation becomes lower than the nonsolar radiation fluxes in the afternoon).

b. Calculation of I_τ.

The wind stress is first computed using the CCMP wind data based on the bulk formulas developed by Fairall et al. (1996b), similar to the approach for nonsolar fluxes, and then the wind stress is divided by the air density ρ to obtain the friction velocity (i.e., momentum fluxes). The term I_τ is the integral of the momentum fluxes during the same time period as I_s.

c. Calculation of the constant (const).

In this paper, we set $\alpha = 2.0 \times 10^{-4}$°C^{-1}, $g = 9.8\,\mathrm{m\,s^{-2}}$, $\mathrm{Ri}_c = 0.65$, $\rho = 1025\,\mathrm{kg\,m^{-3}}$, and $c_p = 3985\,\mathrm{J\,°C^{-1}}$; thus, const $= 9.41 \times 10^{-12}\,\mathrm{m^5\,s^{1/2}\,°C\,kg^{-3/2}\,W^{-3/2}}$.

d. Calculation of ΔT_w.

The term ΔT_w can be estimated using Eq. (B4) after I_s, I_τ, and const are all obtained. As seen in Eq. (B4), the estimation of DSST is basically dependent on $I_s^{3/2}/I_\tau$, which indicates the different effects of heat fluxes and momentum fluxes on the generation of diurnal warming. The heat fluxes, including SWR, LWR, SHF, and LHF, would contribute to developing shallow mixed layer depths and producing large diurnal warming, while the momentum fluxes, which represent mainly wind-induced mixing, would reduce the magnitude of diurnal warming by breaking the mixed layer.

Figure B1 compares the DSSTA estimated using the parameterization and the TAO/TRITON buoy-observed DSSTA in the Niño-3 and Niño-4 regions. In comparison with the buoy observations, the mean biases of the estimated DSSTA are only -3.2×10^{-5}°C and -3.9×10^{-3}°C, respectively, and the correlation coefficients of the estimated values and observations reached 0.73 and 0.82, respectively, in the two regions. Note that there is an underestimation in the amplitude of the DSSTA in the Niño-3 region when compared with observation (Fig. B1a). This may be related to the ocean dynamics that could not be represented in this parameterized model the same as other one-dimensional mixed-layer models. However, its overall interannual variation is consistent with the observation.

Overall, the estimated DSSTA values agreed well with the observations, which indicates that the parameterization is very effective in estimating DSSTA and could be used for further analysis.

REFERENCES

Bernie, D. J., E. Guilyardi, G. Madec, J. M. Slingo, S. J. Woolnough, and J. Cole, 2008: Impact of resolving the diurnal cycle in an ocean–atmosphere GCM. Part 2: A diurnally coupled CGCM. *Climate Dyn.*, **31**, 909–925, https://doi.org/10.1007/s00382-008-0429-z.

Bjerknes, J., 1969: Atmospheric teleconnections from the equatorial Pacific. *Mon. Wea. Rev.*, **97**, 163–172, https://doi.org/10.1175/1520-0493(1969)097<0163:ATFTEP>2.3.CO;2.

Capotondi, A., and Coauthors, 2015: Understanding ENSO diversity. *Bull. Amer. Meteor. Soc.*, **96**, 921–938, https://doi.org/10.1175/BAMS-D-13-00117.1.

Clayson, C. A., and D. Weitlich, 2005: Diurnal warming in the tropical Pacific and its interannual variability. *Geophys. Res. Lett.*, **32**, L21604, https://doi.org/10.1029/2005GL023786.

——, and ——, 2007: Variability of tropical diurnal sea surface temperature. *J. Climate*, **20**, 334–352, https://doi.org/10.1175/JCLI3999.1.

——, and A. S. Bogdanoff, 2013: The effect of diurnal sea surface temperature warming on climatological air–sea fluxes. *J. Climate*, **26**, 2546–2556, https://doi.org/10.1175/JCLI-D-12-00062.1.

Cronin, M. F., and W. S. Kessler, 2002: Seasonal and interannual modulation of mixed layer variability at 0°, 110°W. *Deep-Sea Res. I*, **49** (1), 1–17, https://doi.org/10.1016/S0967-0637(01)00043-7.

Danabasoglu, G., W. G. Large, J. J. Tribbia, P. R. Gent, B. P. Briegleb, and J. C. McWilliams, 2006: Diurnal coupling in the tropical oceans of CCSM3. *J. Climate*, **19**, 2347–2365, https://doi.org/10.1175/JCLI3739.1.

Fairall, C. W., J. S. Godfrey, G. A. Wick, J. B. Edson, and G. S. Young, 1996a: Cool-skin and warm-layer effects on sea surface temperature. *J. Geophys. Res.*, **101**, 1295–1308, https://doi.org/10.1029/95JC03190.

——, ——, E. F. Bradley, D. P. Rogers, J. B. Edson, and G. S. Young, 1996b: Bulk parameterization of air–sea fluxes for Tropical Ocean–Global Atmosphere Coupled Ocean–Atmosphere Response Experiment. *J. Geophys. Res.*, **101**, 3747–3764, https://doi.org/10.1029/95JC03205.

Feng, Y., X. Chen, and K. Tung, 2020: ENSO diversity and the recent appearance of central Pacific ENSO. *Climate Dyn.*, **54**, 413–433, https://doi.org/10.1007/s00382-019-05005-7.

Filipiak, M. J., C. J. Merchant, H. Kettle, and P. Le Borgne, 2012: An empirical model for the statistics of sea surface diurnal warming. *Ocean Sci.*, **8**, 197–209, https://doi.org/10.5194/os-8-197-2012.

Gentemann, C. L., P. J. Minnett, P. Le Borgne, and C. J. Merchant, 2008: Multi-satellite measurements of large diurnal warming events. *Geophys. Res. Lett.*, **35**, L22602, https://doi.org/10.1029/2008GL035730.

Ham, Y., J. Kug, I. Kang, F. Jin, and A. Timmermann, 2010: Impact of diurnal atmosphere–ocean coupling on tropical climate simulations using a coupled GCM. *Climate Dyn.*, **34**, 905–917, https://doi.org/10.1007/s00382-009-0586-8.

Kao, H., and J. Yu, 2009: Contrasting eastern-Pacific and central-Pacific types of ENSO. *J. Climate*, **22**, 615–632, https://doi.org/10.1175/2008JCLI2309.1.

Kawai, Y., and A. Wada, 2007: Diurnal sea surface temperature variation and its impact on the atmosphere and ocean: A review. *J. Oceanogr.*, **63**, 721–744, https://doi.org/10.1007/s10872-007-0063-0.

Lee, T., and M. J. McPhaden, 2010: Increasing intensity of El Niño in the central-equatorial Pacific. *Geophys. Res. Lett.*, **37**, L14603, https://doi.org/10.1029/2010GL044007.

Li, X., T. Ling, Y. Zhang, and Q. Zhou, 2018: A 31-year global diurnal sea surface temperature dataset created by an ocean mixed-layer model. *Adv. Atmos. Sci.*, **35**, 1443–1454, https://doi.org/10.1007/s00376-018-8016-7.

Masson, S., P. Terray, G. Madec, J. Luo, T. Yamagata, and K. Takahashi, 2012: Impact of intra-daily SST variability on ENSO characteristics in a coupled model. *Climate Dyn.*, **39**, 681–707, https://doi.org/10.1007/s00382-011-1247-2.

McPhaden, M. J., 1999: Genesis and evolution of the 1997-98 El Nino. *Science*, **283**, 950–954, https://doi.org/10.1126/science.283.5404.950.

——, 2004: Evolution of the 2002/03 El Niño. *Bull. Amer. Meteor. Soc.*, **85**, 677–696, https://doi.org/10.1175/BAMS-85-5-677.

——, and Coauthors, 1998: The Tropical Ocean–Global Atmosphere observing system: A decade of progress. *J. Geophys. Res.*, **103**, 14 169–14 240, https://doi.org/10.1029/97JC02906.

Reed, R. K., 1977: On estimating insolation over the ocean. *J. Phys. Oceanogr.*, **7**, 482–485, doi:10.1175/1520-0485(1977)007<0482:OEIOTO>2.0.CO;2.

Ren, H., and F. Jin, 2011: Niño indices for two types of ENSO. *Geophys. Res. Lett.*, **38**, L04704, https://doi.org/10.1029/2010GL046031.

Sarachik, E. S., and M. A. Cane, 2010: *The El Niño–Southern Oscillation Phenomenon.* Cambridge University Press, 369 pp.

Soloviev, A., and R. Lukas, 1997: Observation of large diurnal warming events in the near-surface layer of the western equatorial Pacific warm pool. *Deep-Sea Res. I*, **44**, 1055–1076, https://doi.org/10.1016/S0967-0637(96)00124-0.

Stuart-Menteth, A. C., I. S. Robinson, and P. G. Challenor, 2003: A global study of diurnal warming using satellite-derived sea surface temperature. *J. Geophys. Res.*, **108**, 3155, https://doi.org/10.1029/2002JC001534.

Tian, F., J.-S. von Storch, and E. Hertwig, 2019: Impact of SST diurnal cycle on ENSO asymmetry. *Climate Dyn.*, **52**, 2399–2411, https://doi.org/10.1007/s00382-018-4271-7.

Wang, X., C. Guan, R. Huang, W. Tan, and L. Wang, 2019: The roles of tropical and subtropical wind stress anomalies in the El Niño Modoki onset. *Climate Dyn.*, **52**, 6585–6597, https://doi.org/10.1007/s00382-018-4534-3.

Webster, P. J., C. A. Clayson, and J. A. Curry, 1996: Clouds, radiation, and the diurnal cycle of sea surface temperature in the tropical western Pacific. *J. Climate*, **9**, 1712–1730, https://doi.org/10.1175/1520-0442(1996)009<1712:CRATDC>2.0.CO;2.

Wu, Q., 2013: Westerly wind events, diurnal cycle and central Pacific El Niño warming. *Dyn. Atmos. Oceans*, **63**, 79–93, https://doi.org/10.1016/j.dynatmoce.2013.04.002.

Yang, X., Z. Song, Y. Tseng, F. Qiao, and Q. Shu, 2017: Evaluation of three temperature profiles of a sublayer scheme to simulate SST diurnal cycle in a global ocean general circulation model. *J. Adv. Model. Earth Syst.*, **9**, 1994–2006, https://doi.org/10.1002/2017MS000927.

Yang, Y., L. Tim, K. Li, and W. Yu, 2015: What controls seasonal variations of the diurnal cycle of sea surface temperature in the eastern tropical Indian Ocean? *J. Climate*, **28**, 8466–8485, https://doi.org/10.1175/JCLI-D-14-00826.1.

Zhang, H., H. Beggs, X. H. Wang, A. E. Kiss, and C. Griffin, 2016: Seasonal patterns of SST diurnal variation over the tropical warm pool region. *J. Geophys. Res. Oceans*, **121**, 8077–8094, https://doi.org/10.1002/2016JC012210.